Chemical Science

ROYAL SOCIETY OF CHEMISTRY

EDGE ARTICLE

View Article Online
View Journal

Cite this: DOI: 10.1039/d6sc01586g

All publication charges for this article have been paid for by the Royal Society of Chemistry

Received 24th February 2026
Accepted 9th April 2026

DOI: 10.1039/d6sc01586g

rsc.li/chemical-science

Visible-light-induced chlorine photoelimination from acridinium-phosphine gold(III) complexes

Shantabh Bedajna,[a] Kristopher G. Reynolds,[b] Mohammadjavad Karimi,[a] Elishua D. Litle,[a] Daniel G. Nocera *[b] and François P. Gabbaï *[a]

With the objective of developing transition metal complexes that undergo visible-light-induced halogen photoelimination, we have synthesized trivalent gold trichloride complexes featuring an acridinium unit. Photoexcitation of the acridinium chromophore with visible light allows for facile photoreduction to the corresponding Au^{I} complexes, highlighting the photolability imparted by the acridinium moiety onto the Au^{III} centre. The photolysis is remarkably clean, including in the solid state where the photodechlorination is essentially trap-free. Transient absorption spectroscopic studies reveal that the photochemistry is derived from a pathway whereby the S_1 excited state of the acridinium undergoes energy transfer to the Au^{III} center to prompt the photogeneration of Cl radicals.

Introduction

In the past two decades, light-induced processes have found increasing importance in the production of fuels as well as in organic synthesis.[1] Photoinduced halogen evolution in particular has been rigorously investigated as an appealing approach to close the oxidative side of HX splitting cycles.[2] Often referred to as the bottleneck of this energy conversion scheme,[3] chlorine elimination has enjoyed much attention from the scientific community. A number of strategies have thus emerged to investigate this process, with the simplest being exemplified by transition metal complexes, such as **A** and **B** (Fig. 1), which undergo net Cl_2 loss upon photoexcitation to ^{3}LMCT states with weakened M–Cl bonds.[4] High valent gold complexes have also been considered for such processes as described in some of our earlier contributions.[4c,5] For example, $(Ph_3P)AuCl_3$ **C** undergoes photoreduction to its gold monochloride counterpart with quantum yields in the 11–13% range when irradiated at 320 nm.[4c] Based on the notion that such chemistry could, in principle, be driven from an organic chromophore that absorbs near or in the visible range, additional strategies have been considered as in the case of systems of type **D** in which ambient light harvested by the diphenylanthracene chromophore induces photoreduction, even though this process is more efficient upon irradiation at 365 nm.[6]

Building on these precedents, we have started to target platforms that incorporate cationic heteroanthracene moieties. Our strategy rests on the notion that the visible absorption profile of such chromophores would provide a low-energy entrance channel for the targeted photoreductive process. We also speculated that, if placed near the metal centre, such cationic aromatic moieties would preferentially stabilize the low valent form of the metal *via* $[M]\cdots\pi^+$ interactions,[7] providing an impetus for the reduction. In a first implementation of this idea, we recently reported **E**, a gold(III) complex decorated with

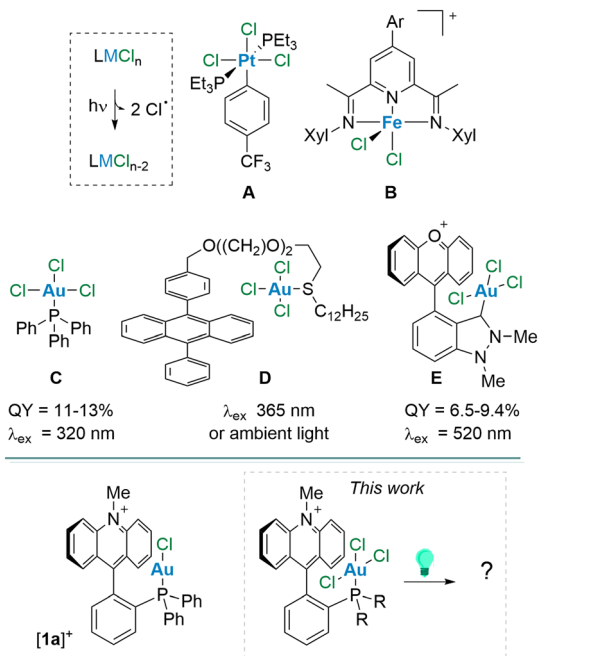

Fig. 1 Top: general photoreductive chlorine elimination and relevant examples of systems that support this transformation. Bottom: structure of a relevant phosphine-acridinium gold complex and graphical representation of the idea explored in this paper.

[a]Department of Chemistry, Texas A&M University, College Station, TX 77843, USA. E-mail: francois@tamu.edu

[b]Department of Chemistry and Chemical Biology, Harvard University, 12 Oxford Street, Cambridge, MA 02138, USA

an adjacent xanthylium unit.[8] We showed that excitation of this derivative, using green light, results in both a xanthylium-centred $\pi \rightarrow \pi^*$ excitation and an intramolecular charge transfer excitation from the indazole backbone to the xanthylium π^* orbital. Access to these two excited states was correlated to the clean dechlorination that ensues at the gold centre.

Aiming to test whether such a strategy could also be implemented in phosphine-based platforms, we have now decided to target phosphine gold(III) complexes that incorporate the *N*-methylacridinium chromophore. This chromophore, which is found in several photocatalysts as originally described by Fukuzumi,[9] is appealing because of its chemical resilience to both reductive[10] and oxidative processes.[11] Moreover, we have already shown that it could be incorporated in phosphine gold(I) derivatives such as $[\mathbf{1a}]^+$,[12] providing a logical starting point for this investigation. In this contribution, we describe our efforts towards the synthesis and photochemistry of trivalent analogs of gold complexes such as $[\mathbf{1a}]^+$ along with an investigation of relevant excited state dynamics using Transient Absorption (TA) techniques.

Results and discussion

Synthesis and structural analysis of the complexes

In addition to using complex $[\mathbf{1a}]^+$ as a starting point for these studies, we also considered its diisopropyl analogue $[\mathbf{1b}]^+$, which was prepared for the purpose of this study (Scheme 1). This new derivative was accessed from 1-lithio-2-diisopropylphosphino-benzene which was quenched with *N*-methylacridone to afford a carbinol (**L**) that was aurated with AuCl(tht) (tht = tetrahydrothiophene) and dehydroxylated using TMSOTf (Scheme 1). Unlike its diphenylphosphino analogue, [**1b**][OTf] is a mildly air-sensitive salt that displays a single resonance in the $^{31}P\{^1H\}$ NMR spectrum at 48.4 ppm, similar to the chemical shift of 51.8 ppm reported for $[(Ph^iPr_2P)AuCl]$,[13] suggesting the formation of the desired cationic gold(I) complex [**1b**][OTf]. Indeed, $^{13}C\{^1H\}$ NMR spectroscopy confirmed the presence of an acridinium moiety characterized by a C9 (C_{carb}) resonance at 160.6 ppm. This value is close to the value of 159.7 ppm reported for $[\mathbf{1a}]^+$.[12a] Single crystal X-ray diffraction analysis of this complex verified the structure of this derivative (Fig. 2), revealing that the AuCl unit is oriented toward the cationic π^+ surface of acridinium, an arrangement also observed for $[\mathbf{1a}]^+$.[12a] The Au–mpln$_{acr}$ and Cl–mpln$_{acr}$ (mpln$_{acr}$ = acridinium moiety mean plane) distances in $[\mathbf{1b}]^+$ at 3.154(4) Å and 3.508(6) Å, respectively, are slightly longer than the analogous distances in $[\mathbf{1a}]^+$ at 3.043(4) Å and 3.318(5) Å. The Au–C_{carb} distance at 3.141(11) Å is slightly shorter than the analogous distance in $[\mathbf{1a}]^+$ at 3.168(9) Å. However, NBO analysis on the optimized structure of this derivative did not reveal any significant interactions between the gold atom and C_{carb}. The observed orientation, with the AuCl moiety upright with respect to the acridinium unit, is most likely the result of favorable electrostatic AuCl$\cdots\pi^+$ interactions[7] as described previously in the case of $[\mathbf{1a}]^+$[12b] and related complexes.[12d]

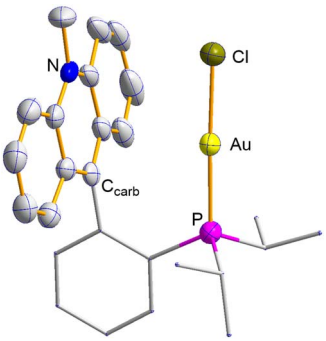

Fig. 2 Solid state structure of [**1b**][OTf]. Thermal ellipsoids are drawn at the 50% probability level and hydrogen atoms and counterions are omitted for clarity. The relevant metrical parameters are in the main text.

The target gold(III) complexes could be conveniently obtained by chlorination of $[\mathbf{1a}]^+$ and $[\mathbf{1b}]^+$ using $PhICl_2$ (Scheme 2). $^{31}P\{^1H\}$ NMR analysis of these reaction mixtures shows quantitative conversion of the gold(I) species and the appearance of new signals at 42.7 ppm and 63.0 ppm for $[\mathbf{2a}]^+$ and $[\mathbf{2b}]^+$, respectively. The chemical shift of $[\mathbf{2a}]^+$ is reminiscent of that reported for $[Ph_3PAuCl_3]$ at 43.9 ppm,[4c] suggesting successful oxidation of the gold centre. $^{13}C\{^1H\}$ NMR analysis of these products indicated the retention of the acridinium unit, noted by a characteristic carbenium signal at 157.3 ppm for both derivatives. Diffusion of Et_2O into concentrated solutions of these salts in MeCN afforded single crystals suitable for X-ray analysis. In the solid state, both complexes show square planar geometry around the gold atom and have similar bond distances (Fig. 3). For $[\mathbf{2a}]^+$ and $[\mathbf{2b}]^+$ the Au–Cl2 bond distance (2.3320(12) Å for $[\mathbf{2a}]^+$ and 2.3328(11) for Å $[\mathbf{2b}]^+$) is slightly longer than the other Au–Cl distances (Au–Cl1 = 2.2723(13) Å and Au–Cl3 = 2.2956(13) Å; for $[\mathbf{2a}]^+$ Au–Cl1 = 2.2869(9) Å and Au–Cl3 = 2.2762(9) Å for $[\mathbf{2b}]^+$), consistent with the more substantial trans influence of the phosphine ligand. The structure of these two trivalent complexes, however, differ

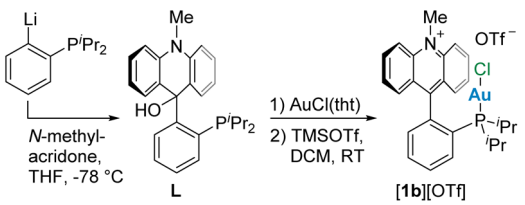

Scheme 1 Synthesis of [**1b**][OTf].

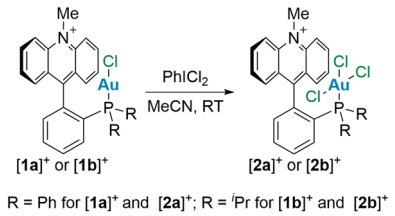

Scheme 2 Synthesis of the gold(III) derivatives.

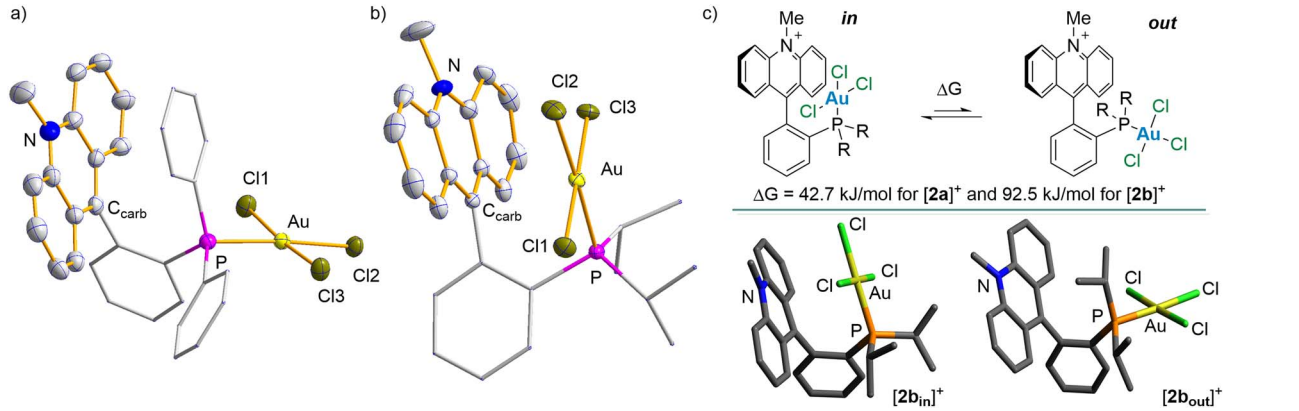

Fig. 3 (a) Solid state structure of [**2a**][BF_4] (b) crystal structure of [**2b**][OTf]. Thermal ellipsoids are drawn at the 50% probability level and hydrogen atoms and counterions are omitted for clarity. (c) "In/out" equilibrium and optimized structures of the two conformers of [**2b**]$^+$ obtained from DFT calculations.

significantly in the orientation of the $AuCl_3$ moiety relative to the acridinium π^+ surface. While the $AuCl_3$ moiety in [**2a**]$^+$ is positioned away from the π^+ system (Cl1–mpln$_{acr}$ distance = 5.625(6) Å, Au–mpln$_{acr}$ distance = 3.991(6) Å), the same fragment in [**2b**]$^+$ retains its upright orientation and remains in contact with the acridinium unit, as indicated by the Au–mpln$_{acr}$ and Cl1–mpln$_{acr}$ distances of 3.2182(19) Å and 3.6525(19) Å, respectively.

This conformational difference prompted us to explore the conformations of these gold(III) complexes computationally. Density Functional Theory (DFT) calculations carried out using the MPW1PW91 functional and a mixed basis set (cc-pVTZ-PP for Au; 6–31G(d′,p′) for P/Cl; 6–31G(d′) for C/N; 6–31G for H) unveiled two local minima corresponding to two conformers with the $AuCl_3$ moiety drawn inward [**2b**$_{in}$]$^+$ or oriented away [**2b**$_{out}$]$^+$ from the acridinium surface (Fig. 3c). Interestingly, the inward conformer [**2b**$_{in}$]$^+$ is 92.5 kJ mol^{-1} lower in Gibbs free energy than the outward conformer [**2b**$_{out}$]$^+$. Similar calculations on [**2a**]$^+$ also revealed two conformers, with the inward conformer [**2a**$_{in}$]$^+$ lying 42.7 kJ mol^{-1} lower in Gibbs free energy than [**2a**$_{out}$]$^+$. These calculations suggest that the smaller energy difference between the two conformers of [**2a**]$^+$ may be more easily overcome by energetically favorable lattice effects, which are elevated by the fact that these complexes are isolated as salts. In either case, the global minimum on the energy surface is the inward conformer with the $AuCl_3$ core situated in the proximity of the acridinium chromophore. This arrangement, which we thought might elevate the lability of the chloride ligands,[14] is reminiscent of that observed in gold complexes featuring boron-based ambiphilic ligands.[15]

Photophysical properties and photochemistry

Eager to investigate this possibility, we decided first to study these complexes by UV-vis spectroscopy. The most salient feature of the spectra of these gold derivatives is the presence of broad low-energy absorption bands in the 390–490 nm region (Fig. 4a and S10–S12). These bands closely resemble those of simple 9-aryl-*N*-methylacridinium compounds,[12b,16] indicating the unambiguous contribution of the acridnium-centred $\pi \rightarrow \pi^*$ excitation to this feature. To support this assumption and identify other possible contributors, we carried out Time Dependent (TD) DFT using the "in" conformers of [**2a**]$^+$ and [**2b**]$^+$. These calculations reveal the primary contributions of two excitations, which both involve the HOMO, LUMO and LUMO + 1 (Fig. S30–S32 and Tables S3–S5) for [**2b**]$^+$. Because the LUMO and LUMO + 1 show dominant acridinium π^* and Au–Cl σ^* ($d_{x^2-y^2}$) character, respectively, the first excitation (E_a) has dominant $\pi \rightarrow \pi^*$ excitation character, while the second one (E_b) has mainly $\pi \rightarrow$ Au–Cl σ^* ($d_{x^2-y^2}$) character (Fig. 4b). Carrying out these calculations on the "out" conformers affords

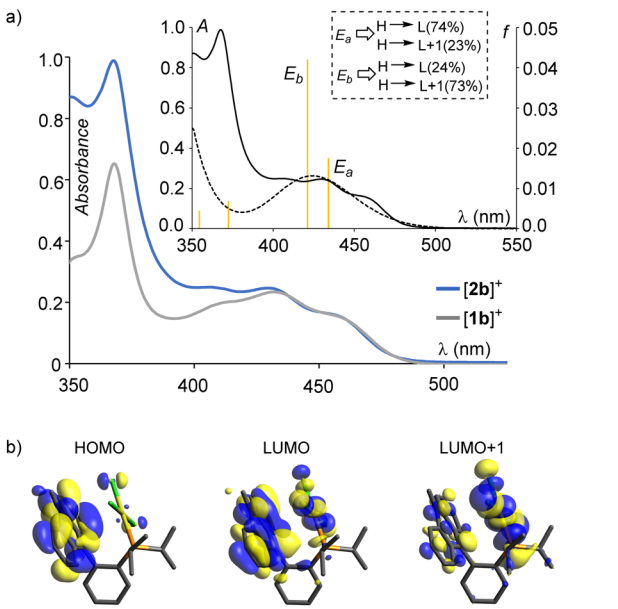

Fig. 4 (a) UV-vis spectra of 1.0×10^{-5} M solutions of [**1b**]$^+$ and [**2b**]$^+$ in MeCN. The inset shows the experimental (solid) and predicted (dashed) UV-vis spectra of [**2b**$_{in}$]$^+$ overlaid with the TD-DFT calculated vertical excitations (yellow bars). (b) Orbitals involved in the vertical excitations (drawn at 0.05 isosurface value).

very similar results, with two low-energy excitations of analogous orbital parentage. These computational findings pose the possibility of $Cl^{\bullet}$ dissociation either by weakened Au–Cl bonds in the excited state due to population of the Au–Cl σ* orbital or by direct energy transfer from the excited acridinium chromophore to the trivalent gold moiety. Addressing these questions may also inform emerging organic synthetic strategies based on gold-centred, light-triggered reductive processes.[17,18]

We next turned our attention to the photochemistry of $[\mathbf{2a}]^+$ and $[\mathbf{2b}]^+$ using a commercial visible light source characterized by a relatively broad illumination spectrum, similar to previous work on hydrohalic acid splitting using non-monochromatic light.[19] The full width at half maximum (30 nm) of this light source, centred at 520 nm, is sufficiently broad to overlap with the low-energy tail of the acridinium absorption envelope of these two compounds (Fig. S13). Irradiation of $[\mathbf{2a}]^+$ and $[\mathbf{2b}]^+$ in MeCN in the presence of 2.5 equiv. of cyclohexene as a chlorine trap resulted in the rapid photoreduction of the gold centre, as indicated by $^{31}P\{^1H\}$ NMR spectroscopy which showed the progressive disappearance of the gold(III) complexes $[\mathbf{2a}]^+$ and $[\mathbf{2b}]^+$ in concert with the emergence of their gold(I) counterparts $[\mathbf{1a}]^+$ and $[\mathbf{1b}]^+$ (Fig. 5, S16 and S17). The photolysis was complete after 20 minutes, and integration of the peaks with respect to the internal standard H_3PO_4, implemented as a sealed capillary in the NMR tube, showed negligible loss of material, indicating that the photoreduction of these complexes is not significantly affected by side reactions. Interestingly, the photolysis of both compounds without a trap proceeds in a clean fashion as well, albeit at a slower rate (Fig. S14 and S15). Encouraged by the resilience of these systems, we selected $[\mathbf{2a}]^+$ for further investigation in the solid state. To this end, $[\mathbf{2a}][BF_4]$ was dissolved in MeCN and drop-cast on a glass slide. While irradiating this compound in air for 60 min followed by dissolution in CD_3CN showed conversion into $[\mathbf{1a}][BF_4]$, signs of photodecomposition were also present. Carrying out the same reaction in a N_2-filled glovebox circumvented this issue, furnishing much cleaner conversion of $[\mathbf{2a}]^+$ into $[\mathbf{1a}]^+$ (Fig. 5, S19 and S20), further documenting the remarkable resilience of the platform. This experiment provides a rare example of solid-state photoreductive elimination of a halogen, with other examples seen in the Fe^{III} complex **B**,[4f] the dimeric Pt^{III}–Pt^{III} complex **F**,[20] the heterobimetallic $[PtSb]^{VII}$ molecule **G**,[21] the dinuclear gold derivative **H**,[4c] and the Ni^{III} system **I** (Fig. 6).[22] These complexes photoeliminate halogen equivalents upon irradiation with higher energy UV light, leading to the formation of undesired decomposition products. Such side reactions appear to be much less

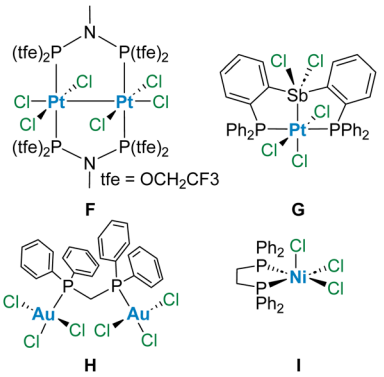

Fig. 6 Known examples of complexes supporting solid state photoelimination of halogens.

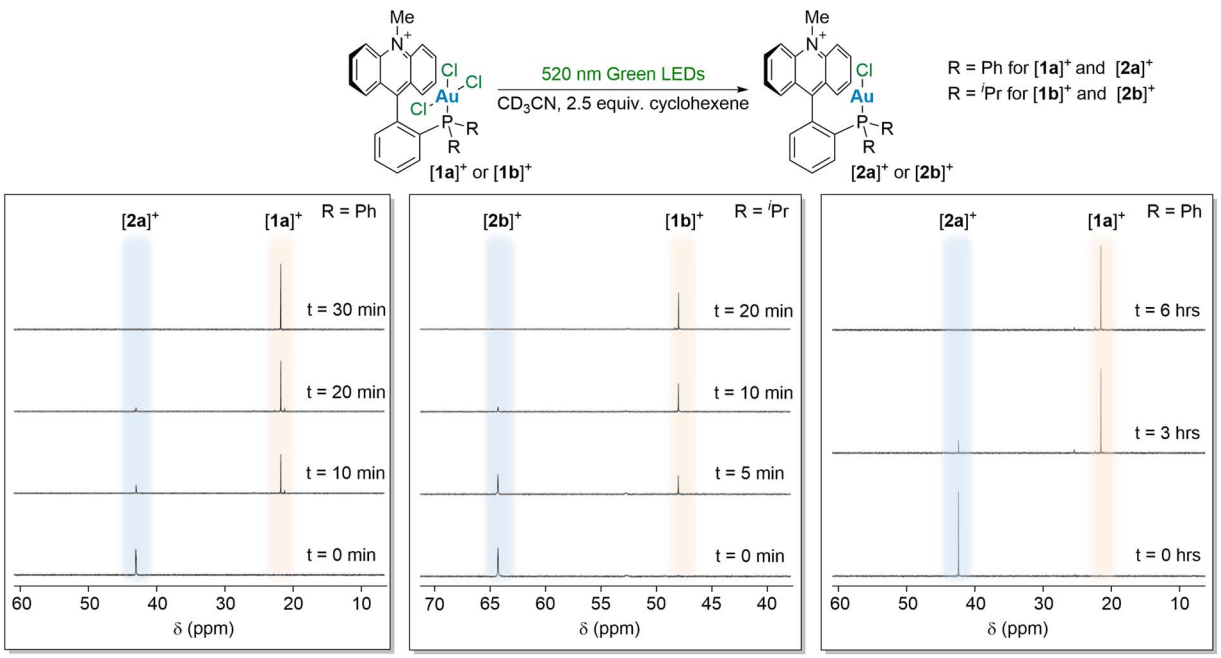

Fig. 5 $^{31}P\{^1H\}$ NMR monitored photoreductive elimination of chlorine from a 0.02 M solution of $[\mathbf{2a}]^+$ (left) and $[\mathbf{2b}]^+$ (middle), both in the presence of 0.05 M cyclohexene as a chlorine trap and H_3PO_4 in a sealed capillary as an internal standard, using 5 W green LEDs as the light source. The right panel shows the $^{31}P\{^1H\}$ NMR monitored photoreductive elimination of chlorine from $[\mathbf{2a}]^+$ in the solid state.

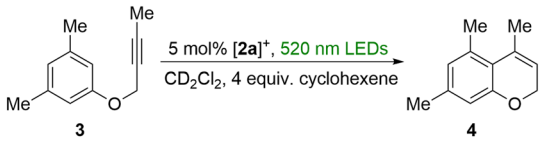

Scheme 3 Gold-catalysed hydroarylation of alkynes turned on by the photolysis of [**2a**][BF_4].

prevalent in the case of [**2a**][BF_4], which, incidentally, might be the only metal platform known to this day to photoeliminate chlorine in the solid state using visible light.

The clean photoinduced dechlorination of [**2a**]$^+$ into [**1a**]$^+$ led us to question whether such a photolysis reaction could be harnessed for light-triggered carbophilic catalysis.[23] The photoevolution of chlorine radicals should produce HCl *via* C–H bond activation of a suitable trap as previously proposed for similar complexes.[8] We questioned whether the released acid and the formation of [**1a**]$^+$ by irradiation of [**2a**]$^+$ would produce a catalytically competent system in which the Au–Cl bond of [**1a**]$^+$ is activated by hydrogen bonding with the released acid.[24] We decided to test this idea using the known intramolecular hydroarylation of **3** as a test reaction.[25] When this compound was irradiated in the presence of [**2a**]$^+$ (5%) and cyclohexene (20%) as a chlorine trap using the above mentioned 520 nm LED light, 47% conversion to the hydroarylation product **4** was observed by ^{1}H NMR after 30 minutes (Scheme 3 and Fig. S26). No catalysis was observed in the absence of light. This simple experiment shows that carbophilic catalysis can be activated by *in situ* photoreduction of [**2a**]$^+$. These results parallel those obtained with complexes such as **D**, which also afford catalytically active systems that readily promote the isomerization of propargyl amides.[6]

Quantum yield measurements with azobenzene as the chemical actinometer[26] and monitored by ^{1}H and ^{31}P NMR spectroscopy (Fig. S21) show that the photoreduction of [**2a**]$^+$ and [**2b**]$^+$ proceeds with quantum yields of 6.1% and 7.9%, respectively, when 2.5 equiv. of cyclohexene is employed. These quantum yields increase to 18.9% and 20.5% when the trap concentration is raised to 25 equiv. (Tables S1 and S2). The elevated magnitude of these quantum yields shows that these systems are among the most active platforms for light-induced chlorine evolution.

These unique photochemical features spark questions about the mechanism of chlorine elimination from the Au(III) platform. There are two possible pathways for net Cl_2 elimination: (i) concerted reductive elimination of a Cl_2 molecule, and (ii) stepwise dissociation of two Cl$^\bullet$ radicals. Our TD-DFT analyses indicate that the radical mechanism is favored (*vide supra*). GC-MS analysis of an irradiated solution of [**2a**]$^+$ in the presence of 10 equiv. of cyclohexene showed formation of 3-chlorocyclohexene as the dominant product (Fig. S18), suggesting the involvement of Cl$^\bullet$ radicals as the main intermediate in the photoreduction. To further delineate the underlying photophysical process leading to chlorine elimination, we examined [**2a**]$^+$ and its photoproduct [**1a**]$^+$ *via* transient absorption spectroscopy on both femto- and nanosecond timescales.

Transient absorption spectroscopy

For context, the photophysics and photochemistry of acridinium dyes have been extensively investigated.[27] The excited state dynamics in acridinium dyes substituted at the 9 position are generally governed by two pathways arising from whether substituents on the dye are able to be oxidized by the acridinium singlet excited state (charge transfer in nature) or not (π localized in nature). The latter exhibits relatively simple photophysics;[28] population of the acridinium-centred singlet excited state is followed by direct return to the ground state, typically by radiative relaxation.[27b] When substituents of the dye are able to be oxidized, rapid charge transfer occurs from the singlet excited state, leading to the formation of the acridinyl radical and the radical cation on the substituent. The absorption spectrum of the resulting acridinyl radical is marked by a characteristic broad band between 500-550 nm. To our knowledge, in all cases where intramolecular charge transfer is observed, charge recombination occurs on the nanosecond timescale to form the acridinium triplet excited state with its subsequent relaxation to the ground state.[27b,28]

To elucidate the excited state dynamics governing the photochemical conversion of [**2a**]$^+$ to [**1a**]$^+$, we first established the photophysics of [**1a**]$^+$, the photoproduct. Fig. S22a shows the femtosecond TA (fsTA) profile of [**1a**]$^+$. Immediately upon excitation (λ_{exc} = 420 nm, 60 nJ), two prominent Excited State Absorptions (ESAs) of the singlet excited state are observed at 395 nm and 480 nm, in addition to a broad ESA extending from 650 nm to the edge of our probe region in the near-infrared (NIR). The bleach feature at 550 nm is attributable to stimulated emission from the singlet excited state. This singlet excited state evolves with a time-constant of 54 ps (Fig. S22b) to the characteristic acridinium triplet excited state, which persists longer than our 6 ns delay line. This localized triplet excited state is captured on our nanosecond TA (nsTA) system (Fig. S22c), and it decays to baseline with a time-constant of 408 ns (Fig. S22d). These data establish that the singlet state of [**1a**]$^+$ undergoes rapid intersystem crossing to the localized acridinium triplet state, mediated by the large spin–orbit coupling induced by the Au(I) centre, followed by straightforward decay to the ground state.

The coordination of P to the gold centre prevents its oxidation by the acridinium singlet excited state. Fig. S23 shows the fsTA spectrum of the ligand species [(*o*-$Ph_2P(C_6H_4)$Acr)]$^+$ ([Acr = 9-*N*-methylacridinium) also referred to as EliPhos.[7] Laser excitation at λ_{exc} = 425 nm produces a prompt TA spectrum that is dominated by the intense absorption signal at λ > 475 nm that is characteristic of the acridinyl radical.[12b] Unbound to gold, the lone pair of P is readily photooxidized by intramolecular electron transfer. We note that the acridinyl radical absorption spectrum is absent in the TA spectroscopy of [**1a**]$^+$, thus establishing that CT does not occur between the singlet excited state and the Au(I) centre.

Femtosecond TA experiments on [**2a**]$^+$ are very similar to those of [**1a**]$^+$. The singlet excited state forms immediately upon excitation (λ_{exc} = 420 nm, 115 nJ) with the same characteristic ESAs at 395 nm and 480 nm and a broad ESA extending from

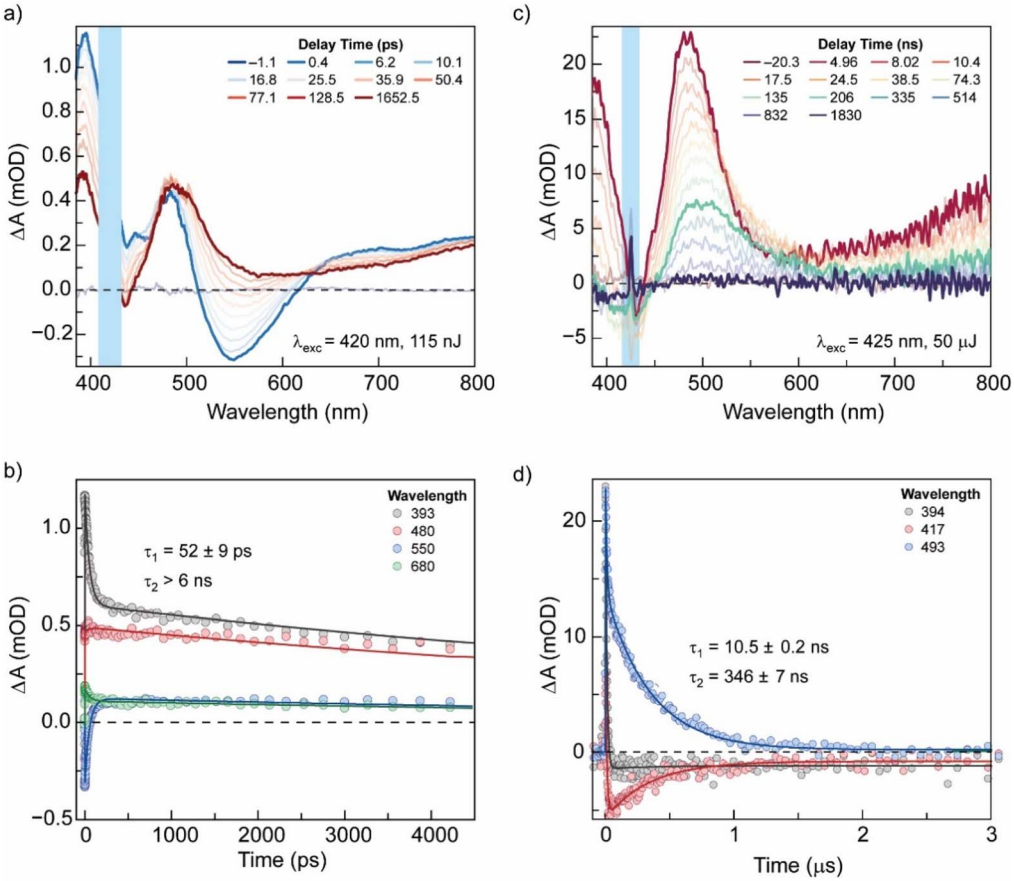

Fig. 7 (a) Femtosecond TA spectra of 114 μM $[\mathbf{2a}]^+$ in MeCN. (b) Femtosecond TA kinetics of $[\mathbf{2a}]^+$ in MeCN. (c) Nanosecond TA spectra of 114 μM $[\mathbf{2a}]^+$ in MeCN. (d) Nanosecond TA kinetics of $[\mathbf{2a}]^+$ in MeCN.

650 nm, along with a stimulated emission feature from the singlet excited state at 550 nm (Fig. 7a). The 52-ps time evolution of the singlet in $[\mathbf{2a}]^+$ (Fig. 7b) is also the same as $[\mathbf{1a}]^+$. However, the fsTA spectra of $[\mathbf{2a}]^+$ notably differ from $[\mathbf{1a}]^+$ in that the 395-nm feature of $[\mathbf{2a}]^+$ is roughly half the intensity of that observed in the TA spectrum of $[\mathbf{1a}]^+$. The spectrum decays with a time constant of 10.5 ns to reveal the triplet excited state, which then decays with its characteristic long lifetime of 346 ns. In contrast to $[\mathbf{1a}]^+$, the nsTA thus establishes the generation of an additional intermediate from the singlet excited state of $[\mathbf{2a}]^+$. The nanosecond TA spectrum of $[\mathbf{2a}]^+$ (Fig. 7c), as in $[\mathbf{1a}]^+$, is that of the localized triplet excited state of acridinium and decays with a time-constant of 345 ns leaving a low intensity permanent bleaching feature between 380–500 nm that resembles the difference absorption spectrum of $[\mathbf{2a}]^+$ and $[\mathbf{1a}]^+$ (Fig. S24), consistent with the photochemical conversion of $[\mathbf{2a}]^+$ into $[\mathbf{1a}]^+$. As was the case in $[\mathbf{1a}]^+$, spectral features of the acridinyl radical, which would result from charge transfer, are absent throughout the entire dataset. Inasmuch as CT is not observed for the more easily oxidized Au(I) centre in $[\mathbf{1a}]^+$, the lack of CT involving the Au(III) centre in $[\mathbf{2a}]^+$ is unsurprising. Focusing on the intermediate uncovered in the 390-nm spectral region, the TA signal at 390 nm is quenched by cyclohexene with a diffusion limited quenching rate constant of $k_q = 1.1 \times 10^9\ M^{-1}\ s^{-1}$ (Fig. S25). Conversely, the lifetime of the triplet excited state, monitored at 483 nm, is unaffected by the presence of cyclohexene. This observation supports the TD-DFT and photochemical analyses (*vide supra*) that Cl˙ is produced as a primary photoproduct, as cyclohexene is a known trap of Cl˙. Accordingly, we believe that the unique intermediate produced from the singlet of $[\mathbf{2a}]^+$, is a dissociated Cl˙ residing in a solvent cage of the gold complex.[29] The decay time constant of 10.5 ns for this species is consistent with observed recombination rates of solvent-caged radicals in polar, organic solvents.[30]

Taken together, our data suggest the Jablonski diagrams shown in Fig. 8 for $[\mathbf{1a}]^+$ and $[\mathbf{2a}]^+$. $[\mathbf{1a}]^+$ shows simple photophysics of acridinium dyes in the presence of a heavy atom to induce intersystem crossing from the excited state singlet to triplet. Excitation of $[\mathbf{2a}]^+$ leads to the population of an acridinium-centred singlet excited state with a rate constant for intersystem crossing that is similar to $[\mathbf{1a}]^+$, as Au(I) and Au(III) are expected to have similar spin–orbit coupling constants. Unlike $[\mathbf{1a}]^+$, however, the singlet decays along a bifurcated pathway in which intramolecular energy transfer from the acridinium triplet to the $Au(III)Cl_3$ centre is competitive with intersystem crossing to lead to the generation of Cl˙ within a solvent cage. We envision the generation of Cl˙ to occur by energy transfer according to two possible pathways: (1) energy

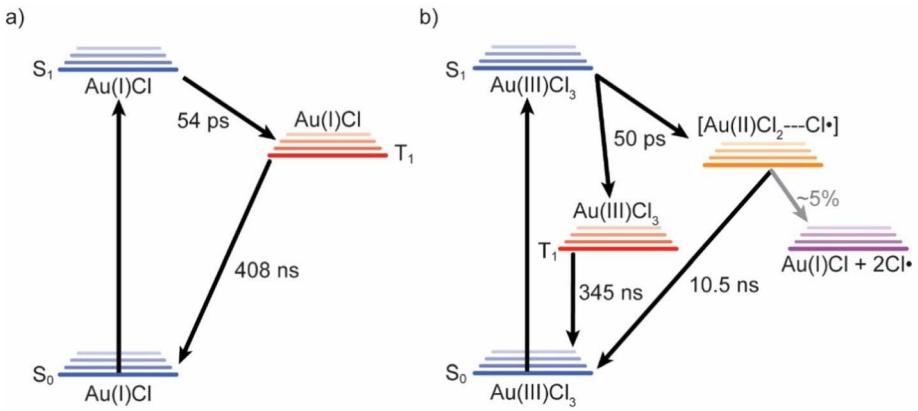

Fig. 8 (a) Jablonski diagram depicting the excited state dynamics of [**1a**]$^+$ (b) Jablonski diagram depicting the excited state dynamics of [**2a**]$^+$.

transfer into a dissociative d–d state to produce Au(III) and Cl^-, which is then subsequently oxidized within the solvent cage to produce [Au(II)$Cl_2\cdots Cl^\bullet$] or alternatively energy transfer to a Au(III)–Cl^- LMCT state to produce [Au(II)$Cl_2\cdots Cl^\bullet$]. Given that neither the acridinium nor the Au(III) centre is sufficiently oxidizing to produce $Cl^\bullet$ from Cl^-, we believe relaxation through a LMCT state is the most likely pathway along which [Au(II)$Cl_2\cdots Cl^\bullet$] forms. As shown in Fig. 7c, this photoproduct dominates the initial nsTA spectrum at early times. Recombination of the radical within the solvent cage pair with a time constant of 10.5 ns reveals the underlying TA spectrum of the triplet excited state. Minor amounts of cage escape leads ultimately to the conversion of [**2a**]$^+$ into [**1a**]$^+$ *via* the loss of an additional $Cl^\bullet$ to result in the complete photochemical transformation.

Identification of energy transfer in [**2a**]$^+$ as the prevailing mechanism for the photochemical production of $Cl^\bullet$ is supported by the lack of a similar reactivity of [**1a**]$^+$. The Au(I) centre of [**1a**]$^+$ obviates energy transfer from the acridinium singlet to the gold centre, as d–d states are not present for a d^{10} electronic configuration. Thus, the Au(I) centre induces intersystem crossing to the triplet state of acridinium as the dominant pathway for the decay of the singlet excited state In contrast, the d^8 electronic configuration of Au(III) enables energy transfer from the acridinium singlet excited state to available d–d states of the Au(III) centre.

Conclusions

In summary, we describe a novel mechanism for the visible light-induced photoelimination of chlorine. Our approach relies on the integration of an acridinium chromophore into the photoredox gold platform, enabling electronic excitation of this π^+ system with visible light. Although previous work on acridinium derivatives is centred on their photoredox characteristics leading to electron transfer from the excited state,[9,11] our TA spectroscopic measurements show that direct energy transfer from the excited state of the acridinium moiety to the trivalent gold trichloride facilitates $Cl^\bullet$ elimination as the key photochemical step. Remarkably, our platform is also well-suited for chlorine elimination in the solid state, with negligible deleterious side reactions during photolysis, highlighting the robustness of the system. Finally, the overall reaction can be leveraged to turn on catalysis at gold, as shown for the hydroarylation of alkynes, *via* photogeneration of the catalytically active mixture.

Author contributions

S. B., E. D. L., K. G. R. contributed equally to this study. E. D. L. carried out the original isolation of [**2a**]$^+$ and surveyed its photoreduction chemistry. S. B. synthesized [**2b**]$^+$ and carried out photoreduction chemistry, quantum yield measurement, trapping studies, computations, and catalytic studies. K. G. R. carried out all TA measurements. M. K. assisted with data analysis, validation, and experiment design. F. P. G. and D. G. N. directed the study. All co-authors participated in the preparation of the manuscript.

Conflicts of interest

There are no conflicts to declare.

Data availability

CCDC 2521156–2521158 contain the supplementary crystallographic data for this paper.[31a–c]

Supporting information (SI): additional experimental and computational details, crystallographic data for all compounds, and *xyz* coordinates of the optimized structures. See DOI: https://doi.org/10.1039/d6sc01586g.

Acknowledgements

The National Science Foundation grants CHE-2154972, CHE-2453754 (F. P. G.) and CHE-2243724 (D. G. N.), the Welch Foundation (A-1423), and Texas A&M University (Arthur E. Martell Chair of Chemistry) (F. P. G.) are gratefully acknowledged for the financial support they provided. Portions of this research were conducted with the advanced computing resources provided by Texas A&M High Performance Research Computing.

Notes and references

1 (*a*) A. Galushchinskiy, R. González-Gómez, K. McCarthy, P. Farràs and A. Savateev, *Energy Fuels*, 2022, **36**, 4625–4639; (*b*) Z. Li, S. Fang, H. Sun, R.-J. Chung, X. Fang and J.-H. He, *Adv. Energy Mater.*, 2023, **13**, 2203019.

2 (*a*) H. B. Gray and A. W. Maverick, *Science*, 1981, **214**, 1201–1205; (*b*) M. D. Brady, R. N. Sampaio, D. Wang, T. J. Meyer and G. J. Meyer, *J. Am. Chem. Soc.*, 2017, **139**, 15612–15615.

3 (*a*) D. G. Nocera, *Inorg. Chem.*, 2009, **48**, 10001–10017; (*b*) L. Troian-Gautier, M. D. Turlington, S. A. M. Wehlin, A. B. Maurer, M. D. Brady, W. B. Swords and G. J. Meyer, *Chem. Rev.*, 2019, **119**, 4628–4683.

4 (*a*) F. David and P. G. David, *J. Phys. Chem.*, 1976, **80**, 579–583; (*b*) D. N. Hendrickson, M. G. Kinnaird and K. S. Suslick, *J. Am. Chem. Soc.*, 1987, **109**, 1243–1244; (*c*) T. S. Teets and D. G. Nocera, *J. Am. Chem. Soc.*, 2009, **131**, 7411–7420; (*d*) T. A. Perera, M. Masjedi and P. R. Sharp, *Inorg. Chem.*, 2014, **53**, 7608–7621; (*e*) R. Fayad, S. Engl, E. O. Danilov, C. E. Hauke, O. Reiser and F. N. Castellano, *J. Phys. Chem. Lett.*, 2020, **11**, 5345–5349; (*f*) D. Gygi, M. I. Gonzalez, S. J. Hwang, K. T. Xia, Y. Qin, E. J. Johnson, F. Gygi, Y.-S. Chen and D. G. Nocera, *J. Am. Chem. Soc.*, 2021, **143**, 6060–6064; (*g*) H. Na, M. B. Watson, F. Tang, N. P. Rath and L. M. Mirica, *Chem. Commun.*, 2021, **57**, 7264–7267.

5 (*a*) T. S. Teets, D. A. Lutterman and D. G. Nocera, *Inorg. Chem.*, 2010, **49**, 3035–3043; (*b*) T. S. Teets, M. P. Neumann and D. G. Nocera, *Chem. Commun.*, 2011, **47**, 1485–1487.

6 (*a*) C. Mongin, I. Pianet, G. Jonusauskas, D. M. Bassani and B. Bibal, *ACS Catal.*, 2015, **5**, 380–387; (*b*) Z. Cao, D. M. Bassani and B. Bibal, *Chem.–Eur. J.*, 2018, **24**, 18779–18787.

7 E. D. Litle, L. C. Wilkins and F. P. Gabbaï, *Chem. Sci.*, 2021, **12**, 3929–3936.

8 G. Park, M. Karimi, W.-C. Liu and F. P. Gabbaï, *Angew. Chem., Int. Ed.*, 2022, **61**, e202206265.

9 (*a*) S. Fukuzumi, K. Ohkubo, T. Suenobu, K. Kato, M. Fujitsuka and O. Ito, *J. Am. Chem. Soc.*, 2001, **123**, 8459–8467; (*b*) S. Fukuzumi and K. Ohkubo, *Org. Biomol. Chem.*, 2014, **12**, 6059–6071.

10 I. A. MacKenzie, L. Wang, N. P. R. Onuska, O. F. Williams, K. Begam, A. M. Moran, B. D. Dunietz and D. A. Nicewicz, *Nature*, 2020, **580**, 76–80.

11 (*a*) N. A. Romero and D. A. Nicewicz, *Chem. Rev.*, 2016, **116**, 10075–10166; (*b*) K. A. Margrey and D. A. Nicewicz, *Acc. Chem. Res.*, 2016, **49**, 1997–2006.

12 (*a*) L. C. Wilkins, Y. Kim, E. D. Litle and F. P. Gabbaï, *Angew. Chem., Int. Ed.*, 2019, **58**, 18266–18270; (*b*) W.-C. Liu, Y. Kim and F. P. Gabbaï, *Chem.–Eur. J.*, 2021, **27**, 6701–6705; (*c*) E. D. Litle and F. P. Gabbaï, *Angew. Chem., Int. Ed.*, 2022, **61**, e202201841; (*d*) W.-C. Liu and F. P. Gabbaï, *Chem. Sci.*, 2023, **14**, 277–283.

13 A. K. H. Al-Sa'ady, C. A. McAuliffe, K. Moss, R. V. Parish and R. Fields, *J. Chem. Soc., Dalton Trans.*, 1984, 491–493.

14 A. J. Neel, M. J. Hilton, M. S. Sigman and F. D. Toste, *Nature*, 2017, **543**, 637–646.

15 (*a*) S. Bontemps, G. Bouhadir, K. Miqueu and D. Bourissou, *J. Am. Chem. Soc.*, 2006, **128**, 12056–12057; (*b*) S. Moebs-Sanchez, G. Bouhadir, N. Saffon, L. Maron and D. Bourissou, *Chem. Commun.*, 2008, 3435–3437; (*c*) G. Bouhadir and D. Bourissou, *Chem. Soc. Rev.*, 2016, **45**, 1065–1079.

16 (*a*) J. Hu, B. Xia, D. Bao, A. Ferreira, J. Wan, G. Jones, II and V. I. Vullev, *J. Phys. Chem. A*, 2009, **113**, 3096–3107; (*b*) J. Eberhard, K. Peuntinger, R. Fröhlich, D. M. Guldi and J. Mattay, *Eur. J. Org Chem.*, 2018, **2018**, 2682–2700.

17 D. Vesseur, S. Li, S. Mallet-Ladeira, K. Miqueu and D. Bourissou, *J. Am. Chem. Soc.*, 2024, **146**, 11352–11363.

18 J. Wu, F. Guo, C. Yi, R. Yang, X. Lei and Z. Xia, *J. Am. Chem. Soc.*, 2025, **147**, 5839–5850.

19 (*a*) M. D. Turlington, M. D. Brady and G. J. Meyer, *ACS Appl. Energy Mater.*, 2021, **4**, 745–754; (*b*) S. A. M. Wehlin, L. Troian-Gautier, A. B. Maurer, M. K. Brennaman and G. J. Meyer, *J. Chem. Phys.*, 2020, **153**, 054307.

20 (*a*) T. R. Cook, Y. Surendranath and D. G. Nocera, *J. Am. Chem. Soc.*, 2009, **131**, 28–29; (*b*) D. C. Powers, S. J. Hwang, B. L. Anderson, H. Yang, S. L. Zheng, Y. S. Chen, T. R. Cook, F. P. Gabbaï and D. G. Nocera, *Inorg. Chem.*, 2016, **55**, 11815–11820.

21 H. Yang and F. P. Gabbaï, *J. Am. Chem. Soc.*, 2014, **136**, 10866–10869.

22 S. J. Hwang, D. C. Powers, A. G. Maher, B. L. Anderson, R. G. Hadt, S. L. Zheng, Y. S. Chen and D. G. Nocera, *J. Am. Chem. Soc.*, 2015, **137**, 6472–6475.

23 S. Witzel, A. S. K. Hashmi and J. Xie, *Chem. Rev.*, 2021, **121**, 8868–8925.

24 (*a*) S. Sen and F. P. Gabbaï, *Chem. Commun.*, 2017, **53**, 13356–13358; (*b*) A. Franchino, À. Martí, S. Nejrotti and A. M. Echavarren, *Chem.–Eur. J.*, 2021, **27**, 11989–11996; (*c*) N. V. Tzouras, A. Gobbo, N. B. Pozsoni, S. G. Chalkidis, S. Bhandary, K. Van Hecke, G. C. Vougioukalakis and S. P. Nolan, *Chem. Commun.*, 2022, **58**, 8516–8519; (*d*) P. Elías-Rodríguez, M. Benítez, J. Iglesias-Sigüenza, E. Díez, R. Fernández, J. M. Lassaletta and D. Monge, *Org. Lett.*, 2024, **26**, 5995–6000.

25 (*a*) M. Alcarazo, *Acc. Chem. Res.*, 2016, **49**, 1797–1805; (*b*) D. You and F. P. Gabbaï, *J. Am. Chem. Soc.*, 2017, **139**, 6843–6846.

26 (*a*) H. J. Kuhn, S. E. Braslavsky and R. Schmidt, *Pure Appl. Chem.*, 2004, **76**, 2105–2146; (*b*) M. Roseau, V. De Waele, X. Trivelli, F. X. Cantrelle, M. Penhoat and L. Chausset-Boissarie, *Helv. Chim. Acta*, 2021, **104**, e2100071.

27 (*a*) K. Kikuchi, C. Sato, M. Watabe, H. Ikeda, Y. Takahashi and T. Miyashi, *J. Am. Chem. Soc.*, 1993, **115**, 5180–5184; (*b*) H. van Willigen, G. Jones and M. S. Farahat, *J. Phys. Chem.*, 1996, **100**, 3312–3316; (*c*) J. W. Verhoeven, H. J. v. Ramesdonk, H. Zhang, M. M. Groeneveld, A. C. Benniston and A. Harriman, *Int. J. Photoenergy*, 2005, **7**, 596840; (*d*) T. Tsudaka, H. Kotani, K. Ohkubo, T. Nakagawa, N. V. Tkachenko, H. Lemmetyinen and S. Fukuzumi, *Chem.–Eur. J.*, 2017, **23**, 1306–1317.

28 G. Jones, M. S. Farahat, S. R. Greenfield, D. J. Gosztola and M. R. Wasielewski, *Chem. Phys. Lett.*, 1994, **229**, 40–46.
29 M. J. Goodwin, J. C. Dickenson, A. Ripak, A. M. Deetz, J. S. McCarthy, G. J. Meyer and L. Troian-Gautier, *Chem. Rev.*, 2024, **124**, 7379–7464.
30 M. Yan, J. C. Lo, J. T. Edwards and P. S. Baran, *J. Am. Chem. Soc.*, 2016, **138**, 12692–12714.
31 (*a*) CCDC 2521156: Experimental Crystal Structure Determination, 2026, DOI: 10.5517/ccdc.csd.cc2qmgmg; (*b*) CCDC 2521157: Experimental Crystal Structure Determination, 2026, DOI: 10.5517/ccdc.csd.cc2qmgnh; (*c*) CCDC 2521158: Experimental Crystal Structure Determination, 2026, DOI: 10.5517/ccdc.csd.cc2qmgpj.